XVI International Conference on Durability of Building Materials and Components
DBMC 2023, China
K.F. Li and D.P. Fang (Eds)

Numerical Simulation on the Pouring Process of Self-compacting Concrete in CRTS III Slab Track

Haonan ZHANG, Yanrong ZHANG, Kai WU and Yi DING

School of Civil Engineering, Beijing Jiaotong University, Beijing 100044, PR China,
22121253@bjtu.edu.cn (Haonan ZHANG), yr.zhang@bjtu.edu.cn (Corresponding author, Yanrong ZHANG), 20115060@bjtu.edu.cn (Kai WU), 22121217@bjtu.edu.cn (Yi DING)

Abstract. *In this study, a fluid-solid coupling model describing the pouring process of self-compacting concrete (SCC) in CRTS III ballastless slab track in straight section was established based on a coupled Eulerian-Lagrangian method, which realized the simulation of the whole pouring process of SCC. The influence law and mechanism of different construction parameters on the pouring process of SCC were studied theoretically. The effects of height and number of funnels on some key indices including the filling rate of SCC, the vertical and lateral displacements of slab track and the forces of withhold were mainly analyzed. The study was aimed at providing theoretical guidance for the intelligent pouring of SCC and the development of intelligent pouring equipment. Results indicated that the higher funnel and double-hole pouring both reduced the pouring time and improved the construction efficiency, and the latter one demonstrated a significant effect. The maximum vertical displacement of track slab was appeared in the middle of slab edge during single-hole pouring but was found in the vicinity of observation hole during double-hole pouring. The maximum lateral displacement of track slab was appeared near the withhold during the pouring process. A higher funnel led to greater pressure of SCC to track slab, which brought about larger vertical and lateral displacements of slab track and higher forces of withhold. Compared to single-hole pouring, the final floating dis-placement and lateral displacement of slab track and the force of withhold were greater during double-hole pouring.*

Keywords: *Self-compacting Concrete, CEL Method, Intelligent Pouring, Pouring Process.*

1 Introduction

Since the first high-speed railway of the world was built in Japan in 1964, high-speed railway develops constantly and plays an important role in the development of economic and convenience of people's transportation. CRTS III slab ballastless track is a kind of track structure with completely independent intellectual property rights in China, which provides a strong technical support for the construction of high-speed railway in China, *the Belt and Road Initiative* and *going abroad strategy* of high-speed railway. Figure 1(a) shows schematic illustrations of CRTS III slab track. The main characteristic of CRTS III slab track is that self-compacting concrete (SCC) is used as the filling layer of the slab track. And the door type rebars below the track slab, SCC and limit groove of concrete base are connected to a whole (Zhang et al. 2013). As the sandwich layer of the track structure, the construction quality of SCC directly determines the durability and service life of slab track (Li et al. 2012).

In the actual construction sites, single-hole pouring is usually selected as the construction metho. And during the pouring process, clamps shown in Figure 1(b) will be installed to prevent the occurrence of the displacements of track slab, which has a negative influence on the regularity of the track slab. To increase the pouring efficiency and guarantee the regularity of the whole track structure, researchers carry out lots of explorations and optimizations for the

construction technology of SCC in the construction sites (Xu et al. 2013, Wang and Li 2015, Wang 2015, Jin 2015, Li et al. 2015, Zhao et al. 2015, Xing 2016, Fan and Tan 2016, Zhang et al. 2020, Zhang and Sheng 2020, Chen 2013). Mengqiang Chen (Chen 2013)verified the reliability and convenience of key construction technologies in the engineering practice, such as “laying track slab first, pouring concrete later; fine mixing slab by slab, pouring slab by slab” and “pouring and forming continuously each track once”. According to engineering experiences, Yanbin Tan (Tan et al. 2017) pointed out that funnel height is the key parameter determining the pouring process of SCC, but the large funnel height is easy to lead to the increase of floating force and the failure of withhold, that is, the fracture of the bolt. Jianhua Zhang (Zhang et al. 2013) advised the pouring height should be 60-80 cm in straight section based on engineering tests to avoid the failure of withhold, the floating of track slab and other problems during the pouring process. So far, the existing research is focused on the summary of construction experiences and the influence law and mechanism of different construction parameters on the pouring process of SCC are rarely studied theoretically.

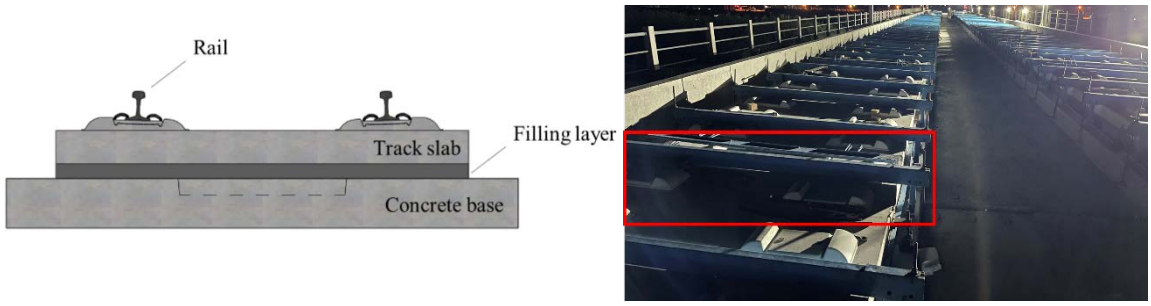

(a) (b)

Figure 1. Schematic illustrations of CRTS III slab track (a) and clamps (b).

In this study, a fluid-solid coupling model describing the pouring process of self-compacting concrete (SCC) in CRTS III ballastless slab track in straight section was established based on a coupled Eulerian-Lagrangian method. And the model realized the simulation of the whole pouring process of SCC, including flowing out of funnel, spreading among the filling layer and filling the whole layer. Based on this model, the influence law and mechanism of height and number of funnels on some key indices including the filling rate of SCC, the vertical and lateral displacements of slab track and the forces of withhold were mainly analyzed, which provided theoretical guidance for the pouring technology of SCC, the development of intelligent pouring equipment and the intelligent construction of slab track.

2 Fluid-solid Coupling Model

Lagrangian method and eulerian method are both fundamental algorithms of continuum mechanics describing the movement of mesh element. Lagrangian method is mainly used for finite element simulation in the field of solid mechanics. However, it will lead to the calculation misconvergence while simulating the large deformation of material due to the distortion of mesh (Hou et al. 2020). And eulerian method is mainly used for the field of fluid mechanics to calculate the extreme deformation of fluid, but it can’t capture the boundary information of the model. CEL method combines the advantages of lagrangian method and eulerian method. This

method not only avoids the distortion of mesh, but also calculate boundaries of material accurately. It is suitable for the model with multiple components and complex topologies and can automatically trace the contact surface between lagrangian and eulerian bodies during the calculation process (Hou et al. 2020). Furthermore, the deformation of eulerian body is represented by the Eulerian Volume Faction (EVF) tool. For an element, if EVF=1, this element is completely filled with eulerian body; if EVF=0, the element is void with no quality or strength; if 0<EVF<1, the element is partially filled with eulerian body. Therefore, the EVF tool can be used to define the initial condition of eulerian body with any shape (Hou et al. 2020).

2.1 Slump Test Model of SCC

2.1.1 Establishment of the model

According to the previous research, the rheological characteristics of SCC can be described with Herschel-Bulkley model (abbreviated H-B model) (De et al. 1998, Zeng 2016). And the material parameters of SCC are given in Table 1 based on literature (Zeng 2016, Lin et al. 2020). Based on these parameters, the quarter finite element model of slump test shown in Figure 2 is established in the finite software ABAQUS, which can simulate the slump and flowing process of SCC.

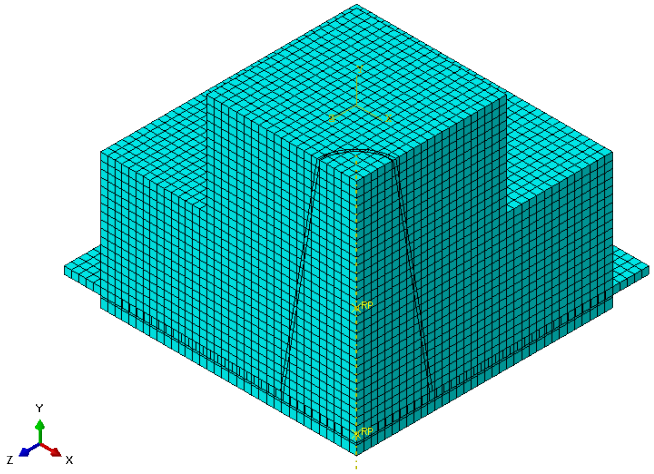

Figure 2. Quarter finite element model of slump test.

Table 1. Material parameters of SCC.

Density / ($kg \cdot m^{-3}$)	Parameters of H-B model			Eos, Us-Up		
	Yield stress / Pa	Plastic viscosity / ($Pa \cdot s^n$)	Flow characteristics index	C_0 / (m/s)	S	γ_0
2370	240	61	1.25	100	0	0

2.1.2 Verification of the model

T_{500} means the time when SCC flows to the distance of 500 mm during the slump test. Table 2 shows the comparisons of T_{500} between simulation and experiments results. And it indicates that the error is only 7.14% when the friction factor is 0.15 between SCC filling layer and concrete base. It can well prove that the accuracy and reliability of the parameters used in the slump test model.

Table 2. Comparisons of results of simulation and experiments on slump of SCC.

Friction factor	Result of test / s	Result of simulation / s	Error
0.1		0.7	87.5%
0.15	5.6	5.2	7.14%
0.25		24.4	335.7%

2.2 Pouring Model of SCC in CRTS III Slab Track

In this study, the CRTS III slab track and pouring equipment of SCC are simulated in full size, and the structure of slab track is partly simplified. This model mainly includes track slab, SCC filling layer, concrete base, withhold and other structures. The size of SCC filling layer is 5.6 m×2.5 m×0.09 m and its parameters are the same as Table 1. SCC is simulated with EC3D8R eulerian element. The size of SCC mesh is 15 mm and the size of dense area is 12 mm. The size of track slab simulated with C3D8R element is 5.6 m×2.5 m×0.2 m and the size of track slab mesh is mainly 25 mm. The size of concrete base simulated also with C3D8R element is 5.65 m×2.9 m×0.2 m and the size of concrete base mesh is mainly 50 mm×50 mm×12.5 mm. And the mesh near the withhold is dense, which is manly 12.5 mm×12.5 mm×12.5 mm. Track slab is C60 concrete and concrete base is C40 concrete. Table 3 shows the material parameters of track slab and concrete base. In addition, the height of limit groove in concrete base is 0.1 m and the size of exhaust hole is 0.09 m×0.09 m. Withhold is simplified to tension and compression bar, which are both simulated with cartesian.

Table 3. Material parameters of track slab and concrete base.

Part	Density / ($kg \cdot m^{-3}$)	Elastic modulus / Pa	Poisson ratio
Track slab	2500	36.5×10^9	0.2
Concrete base	2500	32.5×10^9	0.2

For single-hole pouring, the pouring hole is in the middle of track slab and two observation holes are respectively located on the both sides of pouring hole. And for double-hole pouring, the only observation hole is in the middle of track slab and two pouring holes are respectively located on the both sides of observation hole. Figure 3(a) and 3(b) are the schematic illustrations of the single-hole and double-hole pouring model. Construction equipment includes intrusion pipe, funnel and anti-overflow pipe. The intrusion pipe and funnel are installed at the pouring hole as shown in Figure 3 (c). The inside diameter of intrusion pipe is 0.16 m and its height is 0.4 m. The inside diameter of funnel is 0.76 m. The funnel cylindrical surface heights (abbreviated funnel height) are set to 0.3 m and 0.7 m respectively. And the funnel conical

surface height is fixed at 0.3 m. The anti-overflow pipe is installed in the observation hole. And the inside diameter and overall length of the anti-overflow pipe are 0.16 m and 0.8 m respectively.

General contact is set in the model and contact properties include tangential behavior and normal behavior. Tangential behavior is penalty and the fiction factor is 0.35. Normal behavior is hard contact. To improve calculation efficiency, the quarter finite element model is established in this study. And the symmetry surface is set to symmetry constraint. The bottom surface of concrete base is set to consolidation constraint. It is assumed that the funnel is full of SCC all the time and the initial velocity of SCC is always 0 m/s. In addition, the initial time of pouring process is the time when SCC flows out of the bottom of funnel. And the pouring time is defined as the time required for SCC to flow from the bottom of the funnel to fill the entire filling layer. Figure 3(d) shows the quarter finite element model of pouring of SCC.

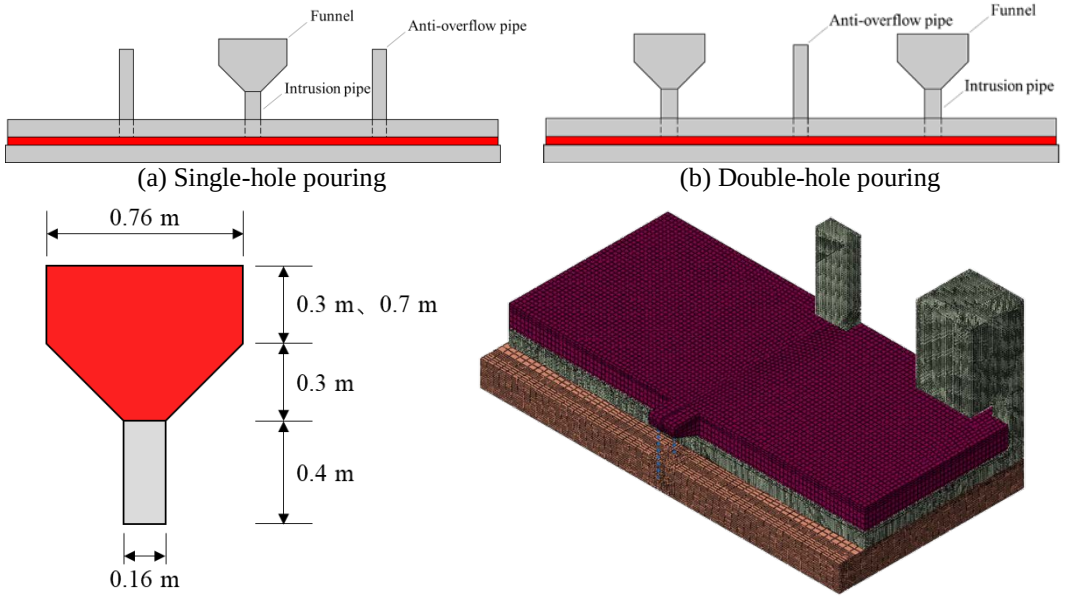

(a) Single-hole pouring (b) Double-hole pouring

(c) Intrusion pipe and funnel (d) Quarter finite element model of pouring of SCC

Figure 3. Schematic illustrations of the model and quarter finite element model of pouring of SCC.

3 Results and Discussions

3.1 Volume Filling Rate

The influence of funnel height on the volume filling rate of SCC is shown in Figure 4(a). As shown in the figure, when the funnel height is increased from 0.3 m to 0.7 m, the volume of SCC in filling layer increases rapidly and pouring time is decreased from 490 s to 310 s, which saves about 37% of pouring time. The influence of funnel number on the volume filling rate of SCC is shown in Figure 4(b). For single-hole pouring, the time required for SCC to fill the filling layer is about 490 s, but double-hole only needs 160 s, which saves about 67.3% of pouring time. It indicated that the increase in the number of funnels can prominently decrease the pouring time and improve the pouring efficiency compared to the increase in the funnel height.

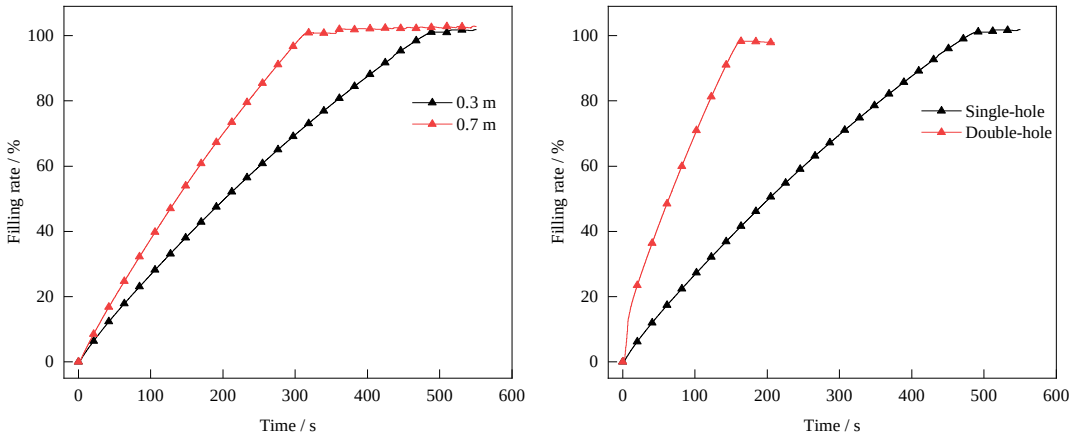

(a) Influence of funnel height (Single-hole) (b) Influence of number of funnels (funnel height: 0.3 m)

Figure 4. Variations of filling rate of SCC during pouring process.

3.2 Displacement of Track Slab

During the pouring process, the flow friction of SCC and the local accumulation of SCC due to the diffusion resistance in the filling layer may lead to the displacement of the track slab in different directions. And the large vertical displacement will lead to the floating of track slab, which will influence the whole track regularity and even endanger the safety of the train.

3.2.1 Influence of funnel height

1) Vertical displacement of track slab

The influence of funnel height on the maximum vertical displacement of track slab is shown in Figure 5. Before the start of pouring, the track slab is slightly sinking under gravity and the maximum vertical displacement is negative. As the pouring proceeds, the maximum vertical displacement remains constant first, then changes to positive values and gradually increases. When the funnel height is 0.3 m, the floating value gradually increases to about 0.22 mm. But it will rapidly increase to about 0.36 mm when the funnel height is 0.7 m.

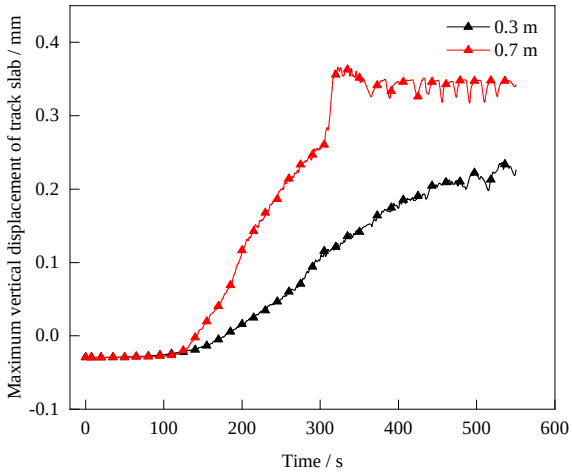

Figure 5. Influences of funnel height on the maximum vertical displacement of track slab.

During the pouring process, the contour plots of vertical displacement of ballastless track in different funnel heights are shown in Figure 6. It can be known from the figure that the maximum vertical displacement of track slab is appeared in the middle of slab edge. This is because that during the pouring process, SCC spreads first to the middle of slab edge, and local accumulation of SCC occurs after being blocked in this position, resulting in the maximum vertical displacement in this area. And the accumulation amount of SCC gradually increases with pouring proceeding, so the vertical displacement of the track slab increases accordingly, which will be constant until the filling layer is basically filled.

Furthermore, the higher funnel height, the larger potential energy of SCC in the funnel. And then the kinetic energy of SCC is larger when it flows out of the pouring hole, which will lead to the greater spreading velocity of SCC in filling layer. Therefore, the accumulation amount of SCC in the middle edge of track slab increases rapidly and the rate of the increase of floating values is greater. In addition, the higher funnel height, the larger the intensity of pressure of SCC on the track slab is larger. So the final floating values are larger.

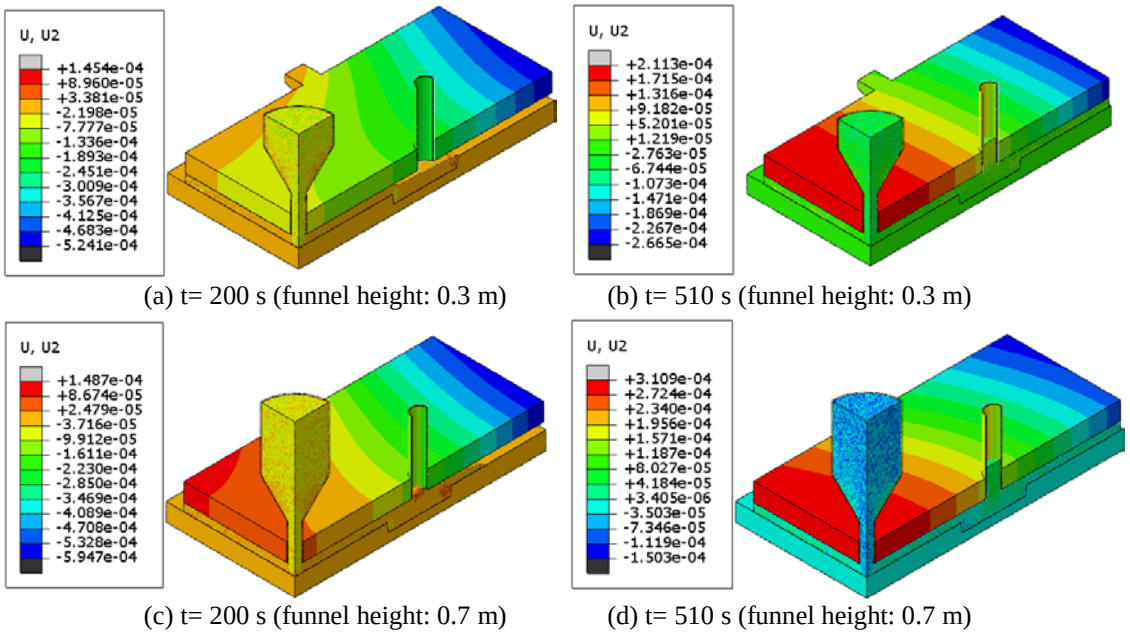

(a) t= 200 s (funnel height: 0.3 m) (b) t= 510 s (funnel height: 0.3 m)

(c) t= 200 s (funnel height: 0.7 m) (d) t= 510 s (funnel height: 0.7 m)

Figure 6. Contour plots of vertical displacement of ballastless track in different funnel heights.

2) Lateral displacement of track slab

The influence of funnel height on the maximum lateral displacement of track slab is shown in Figure 7. According to the quarter finite element model in Figure 3(d), the direction of the funnel center perpendicular to the edge of the track slab is positive, and the opposite direction is negative. Before the start of pouring, lateral displacement of track slab includes positive and negative direction. As the pouring proceeds, the maximum lateral displacement remains constant first, then gradually decreases and increases rapidly after reaching the minimum value and remains basically stable. In the early pouring stage, the maximum value of lateral displacement of track slab basically doesn't change with the funnel height. But the higher funnel height, the greater the rate of the decrease of maximum lateral displacement. When the funnel

height is 0.3 m, the maximum lateral displacement is approximately 0.006 mm in the final. And it is approximately 0.017 mm when the funnel height is 0.7 m.

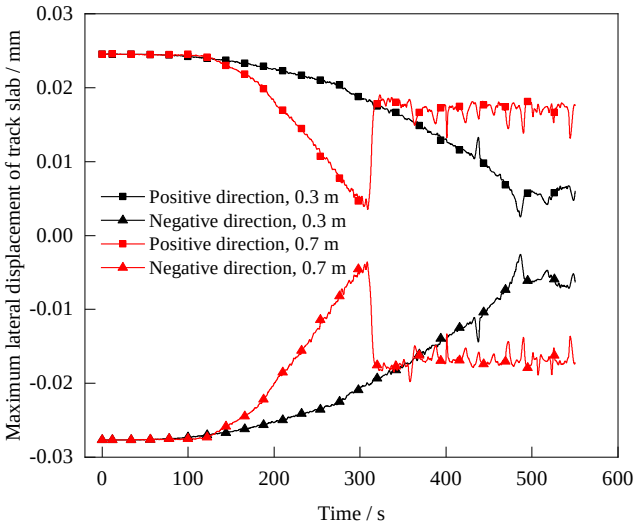

Figure 7. Influences of funnel height on the maximum lateral displacement of track slab.

During the pouring process, the contour plots of lateral displacement of track slab in different funnel heights are shown in Figure 8. It is known from the figure that the maximum lateral displacement of track slab appears near the withhold during the pouring process. The positive and negative maximum lateral displacements in the early pouring stage are located at the upper surface near the tension bars and the lower surface of the track slab respectively, while being located at the lower surface and the upper surface near the tension bars respectively in the later pouring stage. This is mainly due to the fact that tension bars play a role in maintaining the geometry shape and position of track slab during the pouring process, which results in the appearance of the maximum lateral displacement in its vicinity. Furthermore, the higher funnel height, the larger the intensity of pressure of SCC on the track slab after filling layer is full of SCC. Therefore, the finally lateral displacement of track slab is greater when the funnel height is higher.

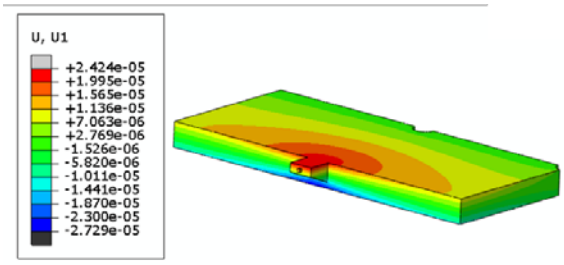

(a) t= 100 s (funnel height: 0.3 m)

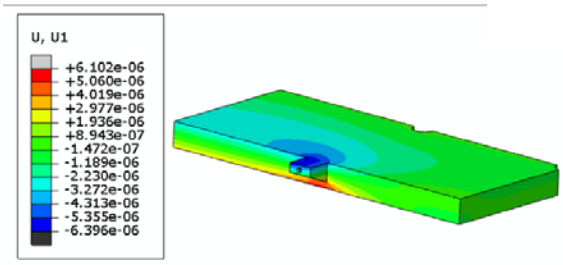

(b) t= 500 s (funnel height: 0.3 m)

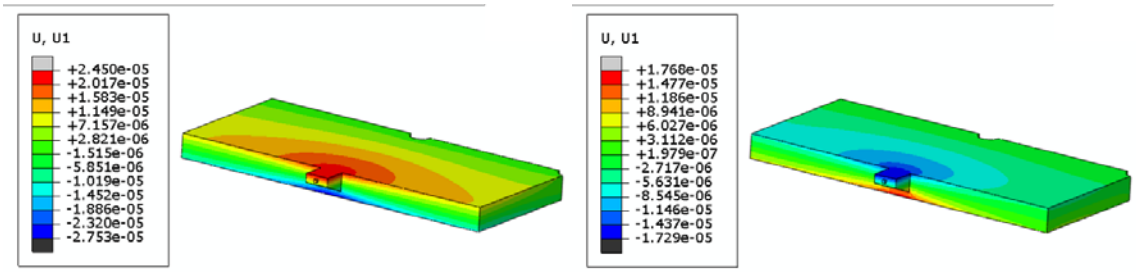

(a) t= 100 s (funnel height: 0.7 m) (b) t= 500 s (funnel height: 0.7 m)

Figure 8. Contour plots of lateral displacement of track slab in different funnel heights.

3.2.2 Influence of funnel number

1) Vertical displacement of track slab

The influence of funnel number on the maximum vertical displacement of track slab is shown in Figure 9. For single-hole pouring, the maximum vertical displacement slowly increases from negative values to about 0.22 mm. However, for double-hole pouring, the maximum vertical displacement first remains constant, then increases to about 0.28 mm rapidly and finally remains basically constant.

The contour plots of vertical displacement of ballastless track in double-hole pouring are shown in Figure 10. Different from the single-hole pouring shown in Fig.6, the maximum vertical displacement mainly appears near the observation hole during the double-hole pouring process. This is because of the fact that when the double-hole pouring is nearly complete, SCC on both sides gathers near the observation hole at a certain flow velocity, and the spreading is blocked. This causes SCC to enter the anti-overflow pipe and drive the track slab to float. It shows that the floating values of the track slab increase rapidly. In addition, the final floating values of double-hole pouring are greater than single-hole pouring. And this is mainly due to the flow friction of a large number of SCC in the anti-overflow pipe.

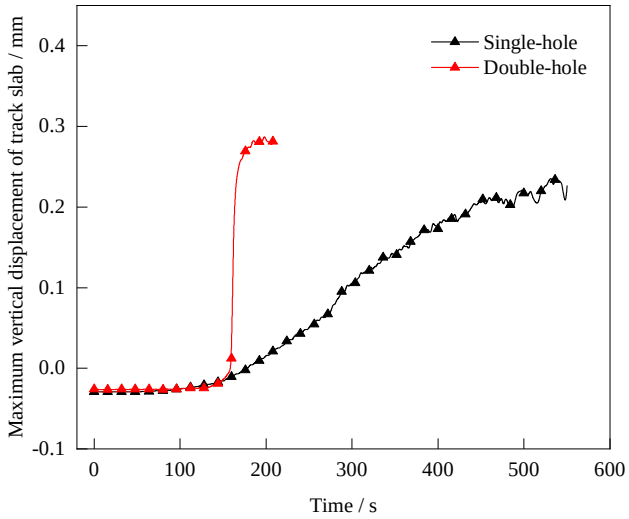

Figure 9. Influence of funnel number on the maximum vertical displacement of track slab.

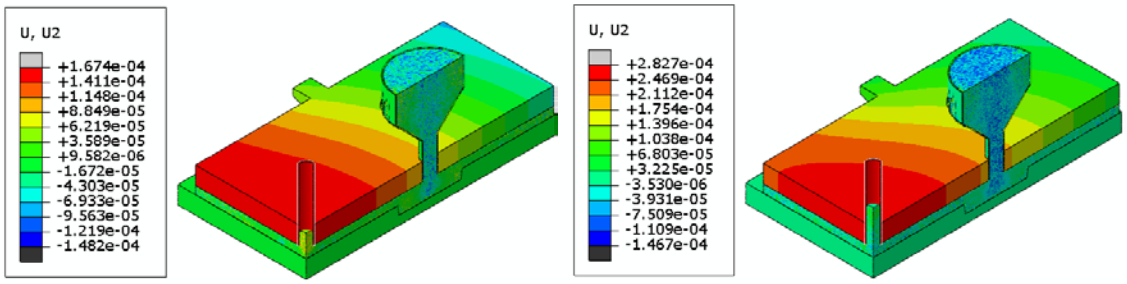

(a) t= 162 s (funnel height: 0.3 m) (b) t= 200 s (funnel height: 0.3 m)

Figure 10. Contour plots of vertical displacement of ballastless track in double-hole pouring.

2) Lateral displacement of track slab

The influence of funnel number on the maximum lateral displacement of track slab is shown in Figure 11. For single-hole pouring, the maximum lateral displacement remains constant first, then decreases to the minimum slowly and increases to about 0.018 mm rapidly in the final. While for double-hole pouring, it remains constant first, then decreases to the minimum rapidly and finally decrease to about 0.018 mm rapidly.

The contour plots of lateral displacement of track slab in double-hole pouring are shown in Figure 12. Similar to single-hole pouring, the maximum lateral displacement also mainly appears near the withhold. And the position of the positive and negative maximum lateral displacements at each pouring stage is consistent with that of single-hole pouring.

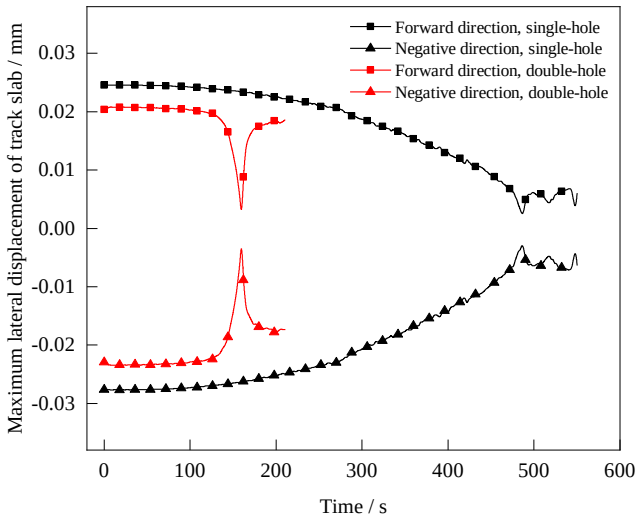

Figure 11. Influence of funnel number on the maximum lateral displacement of track slab.

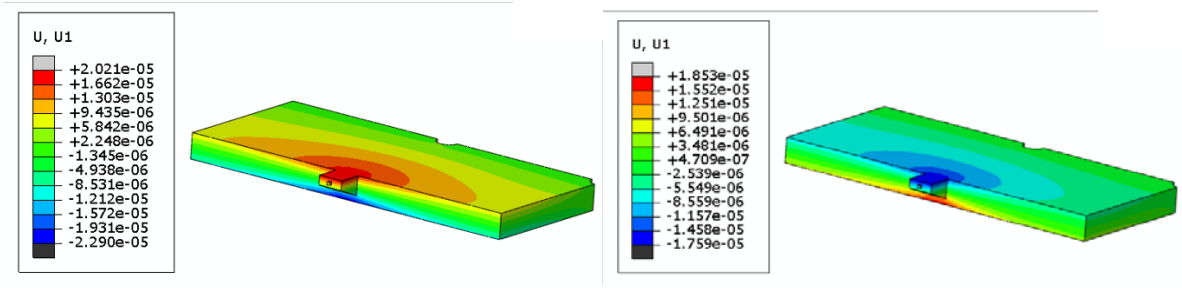

(a) t= 100 s (funnel height: 0.3 m) (b) t= 200 s (funnel height: 0.3 m)

Figure 12. Contour plots of lateral displacement of track slab in double-hole pouring.

3.3 Vertical and Lateral Force of Tension and Compression Bars

As pointed out in the previous paper, the withhold in the model is simplified to tension and compression bar. The tension bar is used to prevent the floating of track slab and the compression bar is used to prevent the sinking of track slab due to its gravity during the pouring process. When the force is too large, the tension and compression bars break and the withhold fails, so it cannot play the role in maintaining the regularity of the track slab.

3.3.1 Influence of funnel height

The influences of funnel height on the vertical force of tension and compression bars are shown in Figure 13(a). Before the start of pouring, the track slab sinks because of its gravity and it is mainly that compression bar is under force. As the pouring proceeds, the vertical force of compression bar gradually decreases to 0 and tension bar begins to play a role. The vertical force of tension bar rises sharply and then remains basically stable. With the increase of funnel height, the time when tension bar is under force is advanced from 180 s to 300 s. And the vertical force of tension bar is significantly increased from about 3.5 kN to about 8.7 kN, increasing to 2.5 times.

According to Figure 5 and 6, the vertical displacement of track slab gradually changes from negative to 0, then to positive and increases to a relatively stable value finally. Correspondingly, the vertical force of tension bar gradually decreases until it is no longer stressed, and the compression force remains at 0. As the pouring proceeds, the track slab appears floating phenomenon, and the tension bar begins to bear force. With the increase of the floating value, the vertical force of tension bar increases rapidly. In addition, the higher the funnel height, the greater the floating value, the greater the rate of the increase of floating value. Therefore, the time when the tension bar bears force is advanced and its vertical force is significantly larger.

The influences of funnel height on the lateral force of tension and compression bars are shown in Figure 13(b). In this figure, the positive and negative represent the direction of the force of the tension bar. The positive is that the tension bar bears the lateral tension, and the negative is that the tension bar bears the lateral compression force. Before the start of pouring, the tension bar bears a large lateral tension. As the pouring proceeds, the lateral tension of tension bar first remains constant, then gradually decreases, and becomes negative after reaching the minimum, then quickly reaches a relatively stable lateral compression force in the final. With the increase of funnel height, the finally lateral compression bar of tension bar is significantly increased from about 2.6 kN to 7.4 kN, increasing to about 2.8 times.

The positive maximum lateral displacement is located at the upper surface near the tension bars, so the tension bar bears lateral tension. However, the negative maximum lateral displacement is located at the upper surface near the tension bars in the later pouring stage, so the tension bar bears lateral compression force at this stage. In addition, the higher the funnel height, the greater the finally lateral displacement of track slab. Therefore, the lateral force of tension bar significantly increases.

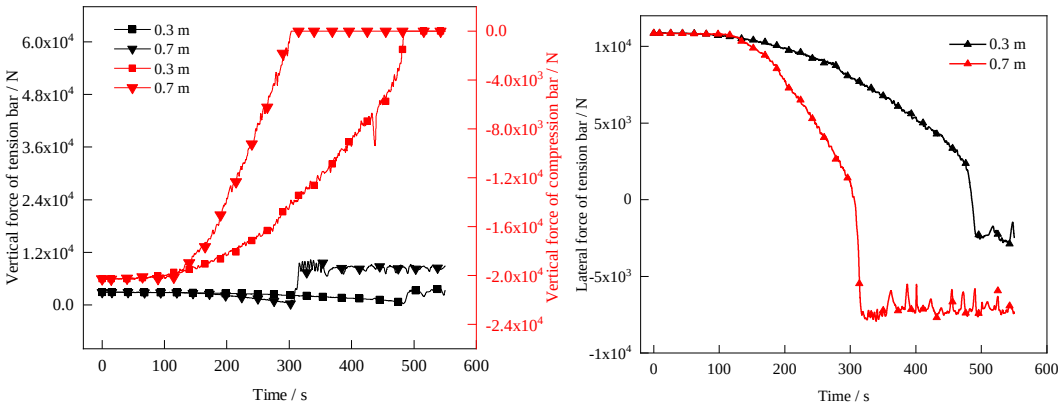

(a) Vertical force of tension and compression bars (b) Lateral force of tension bar

Figure 13. Influences of funnel height on the forces of tension and compression bars.

3.3.2 Influence of funnel number

The influences of funnel number on the vertical force of tension and compression bars are shown in Figure 14(a). Similar to the single-hole pouring, during the double-hole pouring process, the tension bar begins to play a role when the vertical force of compression bar decreases to 0. And the vertical force of tension bar sharply increases. However, different from slow change of the vertical force of the compression bar during the single-hole pouring process, the pressure first remained basically unchanged and then decreased rapidly during the double-hole pouring process. At the same time, with the increase of the funnel number, the time when the tension bar bears force is obviously advanced to about 160 s, and the vertical force of the tension bar is increased from about 3.5 kN to about 8.5 kN, which is increased to 2.4 times.

As mentioned above, the variation law of the vertical force of the tension and compression bars during the pouring process is basically consistent with that of the vertical displacement of the track slab. According to Figure 9 and 10, during the double-hole pouring process, the vertical displacement of track slab first remains constant, then changes to positive values and increases rapidly. So the vertical force of compression bar remains constant first and then decreases to 0 rapidly accordingly. The more the number of funnels, the greater the floating value of the track slab and its growth rate. Therefore, the time when the tension bar bears force is advanced and the vertical force of the tension bar increases obviously.

The influences of funnel number on the lateral force of tension and compression bars are shown in Figure 14(b). Similar to the single-hole pouring, during the double-hole pouring process, the tension bar first bears lateral tension and the force remains constant, then the force decreases and becomes compression force after reaching the minimum, and the compression force reaches to a relatively stable value rapidly in the final. At the same time, with the increase

of the funnel number, the finally lateral compression force of the tension bar increases from about 2.6 kN to about 7.5 kN, increasing to 2.9 times. In addition, the more the number of funnels, the greater the finally lateral displacement of the track slab. So the lateral force of the tension bar increases significantly.

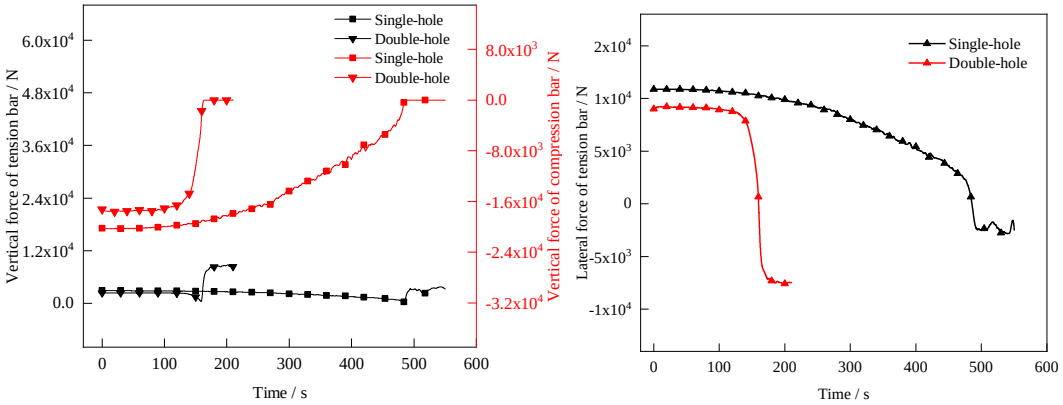

(a) Vertical force of tension and compression bars (b) Lateral force of tension bar

Figure 14. Influences of funnel number on the forces of tension and compression bars.

4 Conclusions

- When the single-hole pouring is adopted, with the height of funnel increasing from 0.3 m to 0.7 m, the pouring time of SCC decreases from 490 s to 310 s, which saves about 37 % of the pouring time. And it only takes 160 s when the double-hole pouring is adopted, which saves about 67.3 % of the pouring time. The increase in the number of funnels can prominently decrease the pouring time and improve the pouring efficiency compared to the increase in the funnel height.
- During the pouring process, the displacement of track slab remains constant first, then the maximum vertical displacement gradually changes from negative values to positive values and the maximum lateral displacement increases rapidly after gradually decreasing to the minimum. The maximum vertical displacement of track slab is appeared in the middle of slab edge during single-hole pouring but is found in the vicinity of observation hole during double-hole pouring. The maximum lateral displacement of track slab is appeared only near the withhold.
- When the funnel height increases from 0.3 m to 0.7 m, the potential energy of SCC increases, the maximum floating value of the track slab increases from about 0.22 mm to about 0.36 mm, the maximum lateral displacement increases from about 0.006 mm to about 0.017 mm, and its growth rate increases significantly. Compared to single-hole pouring, the displacement of double-hole pouring increases rapidly and the final displacement increases, which is mainly due to the flow friction of a large number of SCC in the anti-overflow pipe.
- The variation law of the force of the tension and compression bars during the pouring process is basically consistent with that of the displacement of the track slab. That is, as the pouring proceeds, the vertical displacement of the track slab changes from negative to positive and continues to increase. And the vertical force of the compression bar

decreases to zero, and the compression bar begins to bear the force. The maximum lateral displacement of the upper surface of the track slab changes from positive to negative, and the lateral tension of the tension bar also decreases to the minimum and then changes to the lateral compression force.

- With the increase of the funnel height, the vertical force of the tension bar increases significantly from about 3.5 kN to about 8.7 kN, and the lateral compression force increases significantly from about 2.6 kN to about 7.4 kN. When the double-hole pouring is adopted, the vertical force of the tension bar increases to about 8.5 kN, and the lateral compression force increases to about 7.5 kN.

References

Zhang, J., Li, R. and Liu, Z. (2013). *Study on construction technology of self-compacting concrete filling layer for CRTS III slab track*. China Railway, (12), 33-37.

Li, H., Tan, Y., Xie, Y. and Yi, Z. (2012). *Characteristics and application of self-compacting concrete on high-speed railway*. Railway Engineering, (08), 143-145.

Xu, G., Liu, X., Yang, R., Yang, J. (2013). *Reasons for displacement of ballastless track slab during self-compacting concrete pouring*. Journal of Southwest Jiaotong University, 48(01), 42-46.

Wang, X. and Li, H. (2015). *The withhold technology of track slab for self-compacting concrete construction of CRTS III slab ballastless track*. Railway Construction Technology, (03), 97-101.

Wang, X. (2015). *Discussion on construction technology of self-compacting concrete for CRTS III slab-type ballastless track on Zhengzhou-Xuzhou passenger-dedicated railway*. Railway Engineering, (08), 105-108.

Jin, Z. (2015). *Study on construction technology of CRTS III slab track test section on Xi'an-Baoji high-speed railway*. China Railway, (03), 77-80.

Li, C., Dai, Y. and Gao, J. (2015). *Exposing-plate test and quality control research of self-compacting concrete of CRTS III type slab ballastless track*. High Speed Railway Technology, 6(05), 30-33.

Zhao, Y., Ye, Y., Wang, J., Jiang, C. and Wang, M. (2015). *Research and application on CRTS III slab track system of independent innovation*. Railway Technical Innovation, (02), 40-43.

Xing, X. (2016). *Brief analysis on pouring equipments of self-compacting concrete for CRTS III slab track*. Management & Technology of SME, (03), 94.

Fan, Q. and Tan, Y. (2016). *Optimization and application of construction technology for self-compacting concrete for CRTS III slab ballastless track*. Construction Technology, 45(17), 106-108.

Zhang, J., Liu, X. and Wang, Y. (2020). *Construction quality control of self-compacting concrete for CRTS III ballastless track*. Railway Engineering, 60(08), 143-147.

Zhang, S. and Sheng, M. (2020). *Construction quality control of self-compacting concrete for CRTS III slab ballastless track*. China Railway, (06), 119-125.

Chen, M. (2013). *Key construction technology for self-compacting concrete of CRTS III slab ballastless track*. High Speed Railway Technology, 4(05), 82-86.

Tan, Y., Xie, Y., Yang, L. and Li, L. (2017). *Study and application on self-compacting concrete technology for CRTS III slab track*. China Railway, (08), 21-27.

Hou, Y., Wang, J. and Lu, D. (2020). *Research on the static penetration resistance reduction method of concrete sheet pile based on CEL*. China Rural Water and Hydropower, (6), 154-159.

De, L. F., Ferraris C. F. and Sedran, T. (1998). *Fresh concrete: a Herschel-Bulkley material*. Materials and structures, 31(7), 494-498.

Zeng, S. (2016). *Test method and inversion technique of self-compacting concrete's rheological parameters with L-box based on H-B model*. Hengyang: University of South China. College of Urban Construction, 1-49.

Lin, C. H., Hung, C. and Hsu, T. Y. (2020). *Investigations of granular material behaviors using coupled Eulerian-Lagrangian technique: From granular collapse to fluid-structure interaction*. Computers and Geotechnics, 121, 103485.